RASĀYAN *J. Chem.*
Vol. 18 | No. 4 | 2433-2443 | October-December | 2025
ISSN: 0974-1496 | e-ISSN: 0976-0083 | CODEN: RJCABP
http://www.rasayanjournal.com
http://www.rasayanjournal.co.in

SULFUR/MWCNTS COMPOSITE CATHODE FOR MG-S BATTERY IN AN IONIC LIQUID ELECTROLYTE

S. Rayamma,[1] J. V. Rani[2,✉] and L. Malyala[3]
Polymers and Functional Materials Division, CSIR-Indian Institute of Chemical Technology, Hyderabad, Telangana-500007, India
AcSIR- Academy of Scientific and Innovative Research CSIR Human Resource Development Centre, (CSIR-HRDC) Campus, Ghaziabad, Uttar Pradesh, Pin code-201002, India
Department of Chemistry, National Institute of Technology Warangal, Hanamakonda, Warangal, Telangana, Pin code - 506004, India
✉Corresponding author: vatsala@iict.res.in

ABSTRACT
In this study, we synthesized a sulfur/multiwalled carbon nanotubes (S@CNTs) composite using the melt-diffusion method and applied it as a cathode for the Magnesium-Sulfur (Mg/S) battery. 1-butyl-3-methylimidazolium-tetrafluoroborate ($BMIMBF_4$) with Magnesium bis (Trifluoromethanesulfonyl) imide ($Mg(TFSI)_2$) salt together, aided as an electrolyte for the first time, has led to efficient polysulfide trapping resulting in cycle-life extension and capacity retention. Charging and discharging studies of Mg/S cells with an S@CNTs cathode and a Mg anode showed a columbic efficiency of 95% and reversibility with a capacity of 386 mA h/g. The cell exhibited significant cyclic stability over 100 cycles and an 86.5% capacity retention. S@CNT formation validated by the X-ray diffraction (XRD), field emission scanning electron microscopy (FESEM), and energy dispersive X-ray (EDX) examination. This work presents preliminary results on a Magnesium-Sulfur (Mg/S) electrochemical device with an S@CNTs composite cathode.
Keywords: S@CNTs Composite, Magnesium Electrodes, Mg $(TFSI)_2$, $BMIMBF_4$ Ionic Liquid Electrolyte.
RASĀYAN *J. Chem.*, Vol. 18, No. 4, 2025

INTRODUCTION

Nowadays, major issues like the greenhouse effect, fossil fuel depletion, and pollution have attracted everyone's attention toward energy storage materials and their derivatives.[1-4] Innumerable metal-ion batteries have been developed, but lithium-ion batteries (LIBs) are effective for energy storage in numerous technologies in the electronic markets. The main drawbacks of LIBs are lithium scarcity, thermal runaway, and dendrite formation, which can lead to short-circuit explosion. By this, there is an immediate need to find an alternative to the LIBs. Among alternative technologies, rechargeable magnesium ion battery (RMIB) is regarded as the ideal substitute for LIBs, because of its abundance, non-toxicity,[5] high theoretical volumetric capacity (3832 mA h/cm^3), high negative reduction potential (-2.35 V), and does not form dendrites like lithium.[6] Among various cathodes, sulfur would be a viable cathode for RMIB because of its theoretically high specific capacity of 1672 mA h/g over a two-electron reduction process per atom. The RMIB with a sulfur cathode and magnesium anode has 3200 Wh/L theoretical volumetric energy density; this is more than the lithium-sulfur battery's density, which is 2800 Wh/L.[7, 8] This combination confers high volumetric energy density (1684 Wh/kg) to the Mg-S system.[9-11] The electrochemical reaction between magnesium and sulfur is the basis for how Mg-S batteries work, i.e., $S_8 + 8Mg^{2+} + 16e^- \leftrightarrow MgS$.[10,12-14] The ionically and electronically insulating nature, the quick fading capacity of sulfur, and the short life span of the product polysulfide[15-17] in the electrochemical process due to high solubility, and also in the redox shuttle mechanism are the challenges to be resolved.

Hence, supplementing the cycling execution and revamping the sulfur usage are salient factors concerning the comprehension of high-energy Mg-S batteries. To increase the sulfur cathodes' electrical conductivity and stop the cycling-induced loss of soluble polysulphide intermediates,[18,19] the conductive carbon, MWCNTs, graphene, carbon hollow spheres, CNT/graphene hybrids, and CNT@micro/meso-porous are used to synthesize advanced composite cathodes with high conductivity, strong electron/ion pathway,

http://doi.org/10.31788/RJC.2025.1849278

preferable reversible charge–discharge capacity, and cycling performance.[20] In the present work, sulfur-MWCNTs composite was prepared and utilized as a cathode for Mg-S batteries. Apart from suitable cathode materials, the accessibility of appropriate electrolytes possessing ionic conductivity is also very crucial, wherein Mg ions could deposit reversibly. Imidazolium-based ionic liquids have good ionic conductivity due to imidazolium cations. As diffusion coefficients of ILs with cations are greater than those of anions, the conductivity turns on the mobility of cations; therefore, ionic liquids have a special worth as electrolytes when compared to organic solvents. Due to its electrophilic properties,[21] sulfur was effectively paired with the ionic liquid 1-butyl-3-methylimidazolium-tetrafluoroborate ($BMIMBF_4$), which serves as an optimal electrolyte owing to its non-nucleophilic characteristics,[22] it not only conducts Mg-ions but also stabilizes sulfur. Ionic liquids with BF_4^- have high conductivity, low viscosity, low melting point, and exhibit a good stable electrochemical potential window and magnesium deposition–dissolution efficiency.[23] S. Kim *et al*. proposed a $BMIMBF_4$ electrolyte for Li-S cells with high discharge capacity.[24,25] The dissolution and deposition of Mg in $BMIMBF_4$ using $Mg(CF_3SO_3)_2$ salt was studied and was not viable for long-term cycles due to high overpotential.[26,27] In this work, we utilized $Mg(TFSI)_2$ salt, which is found to be a good choice to pair with $BMIMBF_4$ due to its high stability, the electrochemical stability window is quite large, the ionic conductivity is high, and it is compatible with magnesium metal anodes.[28] Here, we demonstrate the functionality of Mg−S cells using a non-nucleophilic Mg-electrolyte ($BMIMBF_4$+$Mg(TFSI)_2$) and an advanced cathode structure. MWCNTs and sulfur (S@CNTs) active material are used in the cathode to increase the cell's cyclability. The charge-discharge cycles of Mg-S batteries are also studied using spectroscopic and electrochemical methods.

EXPERIMENTAL

Materials

High-purity Sulfur (99.98%), Magnesium powder (99%), and poly (vinylidene fluoride) (PVDF), Bromo butane (99%), N-methyl imidazole, N-methyl pyrrolidine (NMP) (99.5%), and Multi-Walled Carbon Nanotubes (MWCNTs), Magnesium bis (trifluoro methane sulfonyl) imide, (Mg $(TFSI)_2$) were procured from Sigma-Aldrich. Acetonitrile (CH_3CN), Dichloromethane (CH_2Cl_2), and Sodium tetrafluoro borate ($NaBF_4$) (98%) were purchased from Finer and Avra chemicals. Super-p (99.9%) has been procured from Alfa-Aesar, India.

Synthesis of Sulfur/MWCNTs (S@CNTs) Composite

The cathode was synthesized by using elemental sulfur powder and MWCNTs in the weight ratio of 8:2 by mixing them homogeneously by using a mortar and pestle for two hours at an ambient temperature. The solution moved into a pressure vessel, which is a glass tube that has been sealed, and heated at 155 °C in an argon atmosphere for eight hours to obtain sulfur/MWCNTs (S@CNTs) composite. The sulfur melts and diffuses onto a conductive network of MWCNTs during the S@CNTs composite synthesis process. The schematic representation of the synthesis of the S@CNTs composite is shown in the supplementary information (Scheme-1). The composite formation is further confirmed by structural characterizations (XRD, FESEM, EDS, TGA, and XPS analysis). The electrochemical activity was observed by assembling a flooded cell using the S@CNTs cathode and Mg anode.

Synthesis of Ionic Liquid $BMIMBF_4$

A mixture of 1-methyl imidazole (4.15g, 50 mmol) and n-butyl bromide (8.22 g, 60 mmol) was mixed in a round-bottom flask along with a definite amount of acetonitrile solvent and stirred for 3 days at 70 °C. Subsequently, the reaction mixture was unglued to terminate the excess bromoalkane, giving 1-butyl-3-methylimidazolium bromide (BMIMBr). Further BMIMBr and $NaBF_4$ with equivalent molar amounts (1:1.2) were mixed in acetone and stirred for 1 day at 25 °C. Then the reaction mixture was filtered to remove precipitated bromide salt (NaBr). In the end, the obtained solvent was evaporated to yield $BMIMBF_4$. Further, $BMIMBF_4$ was dissolved in dichloromethane (CH_2Cl_2, 50 mL) to extract the impurities, followed by a deionized water wash several times. The resultant aqueous solution was washed with silver nitrate ($AgNO_3$) till no precipitate formed, signifying that no residual bromide was present, and the organic layer containing $BMIMBF_4$ was evaporated to remove CH_2Cl_2. Ultimately, the purified $BMIMBF_4$ was obtained after drying overnight under vacuum at 120 °C. The schematic representation of

the synthesized electrolyte was shown in the supplementary information (Scheme-2). The synthesized $BMIMBF_4$ was confirmed by ^{1}H-NMR and ^{19}F-NMR, as shown in the supplementary information (Fig.-S1, S2). Later, Mg $(TFSI)_2$, a magnesium salt, was added to $BMIMBF_4$ ionic liquid to prepare a 0.10 M concentrated electrolyte and stirred for nearly 6 h at RT.[29]

Fabrication of an Anode

Magnesium powder (90%), PVDF (5%), and super-p (5%) were pulverized to attain a homogeneous mixture, and NMP was added slowly to make a viscous slurry. Thus, the obtained slurry was applied on a silver-copper mesh (area: 0.4cm^2) and oven-dried for 12 h at 120 °C.

Fabrication of Cathode

S@CNTs composite cathode was prepared by using MWCNTs (80 wt% %), super-p (10 wt% %), and PVDF (10 wt% %), which was added gradually and crushed to make a fine slurry, and then solvent (NMP) was added. Finally, the coating of slurry on stainless steel mesh was dried for 12 hours at a temperature of 100 °C before it was utilized.

Material Characterizations

The characterization and chemical analysis of S@CNT composites were illustrated using X-ray Diffraction (XRD Model PIXEL-3D detector, source: Cu Kα = 1.5404 Å). Studies on the microstructure and the distribution of elements were carried out using a Field Emission Scanning Electron Microscope (FE-SEM) (JEOL@7610) that had an OXFORD installed. Energy Dispersive Analysis of X-ray (EDAX) detector, Transmission electron microscopy (TEM) analysis was performed on FEI Talos F200X HR-TEM operating at 120 kV. The thermal stabilities of the samples were assessed utilizing a TA Q 50 thermo-gravimetric analyzer (TGA) between 25°C and 800°C in an inert atmosphere, at a ramp rate of 10 °C/min. X-ray photoelectron spectrometry (XPS) using a Kratos Axis Supra device was used to investigate the chemical environment of the composite cathode material. UV-Vis spectroscopy was used on a Lambda 950 PerkinElmer to analyze the electrochemical mechanisms.

Electrochemical Characterization Studies

Assembled half and complete Mg-S cells were evaluated for their electrochemical performance using electrochemical impedance spectroscopy (EIS), galvanostatic charge-discharge (GCD), and cyclic voltammetry (CV) studies using Origalys, model VSP workstation. Mg/S test cells were constructed using S@CNTs composite as cathode, Mg powder coated on silver-coated copper mesh as anode, 0.1 M $BMIMBF_4$+Mg$(TFSI)_2$ as electrolyte, and cellulose as separator; all the electrochemical studies were performed. The CV and GCD studies were carried out at a 0.0 to 2.2 V vs. Mg/Mg^{+2} potential window. EIS studies were performed at open-circuit potential in a 20 kHz to 100 mHz frequency range at 5 mV amplitude.

RESULTS AND DISCUSSIONS

Material Characterization

An XRD study was performed to explore the S@CNTs composite's crystal structure (Fig.-1a). The S@CNTs composite's XRD spectra exhibit noticeable sulfur peaks similar to the peaks of the elemental sulfur (JCPDS 08-0247), suggesting that no phase transformation and changes in the orthorhombic crystal structure of the sulfur occurred during composite formation. Further, it also observed that in the composite the peak at 26^o corresponding to MWCNTs is found to be disappeared and other peaks of the composite are slightly enhanced at 26^o indicates that the sulfur is well embedded onto the surface of MWCNTs.[15, 30] TGA analysis of pure sulfur and S@CNTs composite were performed under an inert atmosphere at 50 to 600 ^{o}C to estimate the amount of sulfur present in the S@CNTs composite (Fig.-1b). The sulfur evaporation in pure sulfur was observed at 150 ^{o}C and completed at 340 ^{o}C. The TGA study showed that the composites' sulfur content for the S@CNTs is 81.45 %. From the S@CNT composite's TGA curve, it was observed that the sulfur started to rapidly lose weight at 180 °C and lost all of its weight at 315 °C. As per the TGA curve of the S@CNTs composite, the sulfur exhibited a rapid weight loss starting at 180 °C and completely lost its weight at 315 °C. Results indicate that the S@CNTs composite loses around 81.3% of its weight, which means that the composite's sulfur content is 81.3 % consistent with the theoretical Figure.[15, 31]

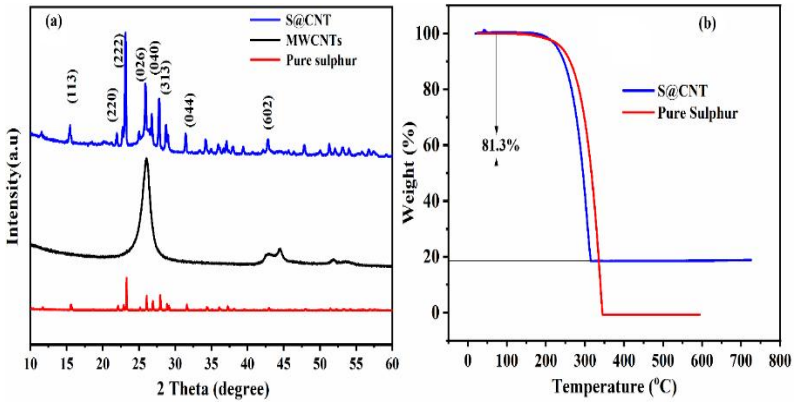

Fig.-1: (a) XRD Spectra of Pure Sulfur, MWCNTs, and S@CNTs Composite, (b) TGA Curves of Pure Sulfur and S@CNTs Composite

The structural and morphological changes of the S@CNTs composite were examined by FESEM and TEM analysis. Figure-2a of bare MWCNTs reveals that tube-like structures are interwoven together to form a porous network structure.[32] Figure-2 (b-d) presents the FESEM images of the S@CNTs at low and high magnifications, which demonstrate that after wrapping the sulfur onto the MWCNTs, the morphology of the composite doesn't change, and it's easy to see that the sulfur is spread out evenly on the MWCNTs' surface, which indicates the successful formation of the composite.[33] TEM image (Fig.-2e) also demonstrates that the surface of individual composite nanotubes becomes coarser, suggesting that sulfur has been successfully loaded onto the surface of MWCNTs. Additionally, no isolated sulfur particles are found, indicating that the surface of MWCNTs is covered with a uniform and continuous sulfur film in the form of a tubular layer.[15,34] Further, EDX analysis with elemental mapping was performed (Fig.-2f) to confirm the composite formation. The steady signal of sulfur and carbon indicates that the sulfur is distributed uniformly. In support of EDX analysis, XPS measurements are conducted in order to examine and comprehend chemical interactions between the O, C, and S elements present in the S@CNTs cathode (Fig.-7). The wide spectrum of S@CNTs shows peaks corresponding to sulfur, carbon, and oxygen, respectively (Fig.-7a). Two strong peaks at 165.1 and 163.8 eV, which correspond to S 2p1/2 and S 2p3/2 of elemental sulfur, respectively, are visible in the high-resolution S 2p spectra of S@CNT (Figure 7b), respectively, are visible in the high-resolution S 2p spectra of S@CNTs (Fig.-7b).[5,35] The peak at 163.8 eV suggests the potential presence of a C-S bond as the BE is marginally lower than the elemental sulfur (164.0 eV).[36, 37]

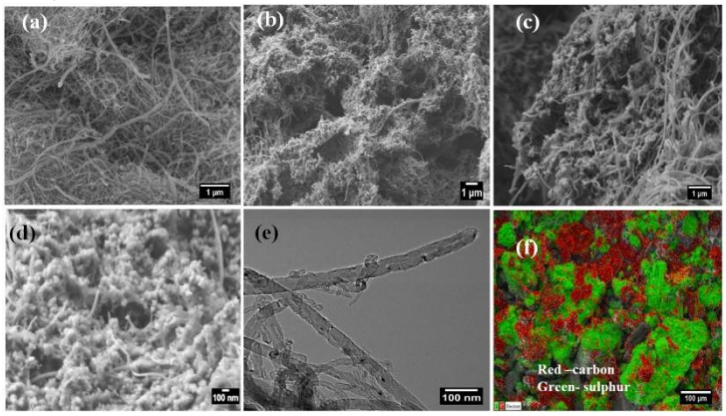

Fig.-2: FESEM Images of (a) MWCNTs, (b-d) S@CNTs at Low and High Magnifications, (e) TEM Image, and (f) Elemental Mapping of S@CNTs Composite

Electrochemical Characterization

Cyclic Voltammogram of Mg Half-cell

To analyze the reversibility of Mg dissolution and deposition, CV studies are predominantly performed by setting up a 3-electrode cell with Mg electrodes used as both a standard and a counter, a Pt plate with

0.1 M BMIMBF4+Mg(TFSI)2 electrolyte as a working electrode, respectively. The CV was recorded within -1 to 2.0 V potential window vs Mg/Mg^{2+} (Fig.-3). The CV profile at 5 mV/s scan rate (Fig.-3a) demonstrates two prominent oxidation and reduction peaks at 0.89 V, 1.5V, and 0.5, -0.25 V, respectively, corresponding to Mg dissolution and deposition. When the scan rate was altered from 1 to 10 mV/s, Oxidation and reduction peaks were observed; the redox peaks moved to higher and lower potentials, respectively (Fig.- 3b). Nonetheless, the current ascribed to the Mg-salt containing $BMIMBF_4$ is exceedingly prominent in either peak. After a few cycles, the reversible cycling efficiency of Mg deposition/dissolution continues; there was no decrease in peak positions following fifteen cycles of reversible scanning. These findings indicate that the dissolution/deposition of Mg demonstrates the mobility of Mg^{2+} ions in the 0.1 M $BMIMBF_4$+$Mg(TFSI)_2$ electrolyte.

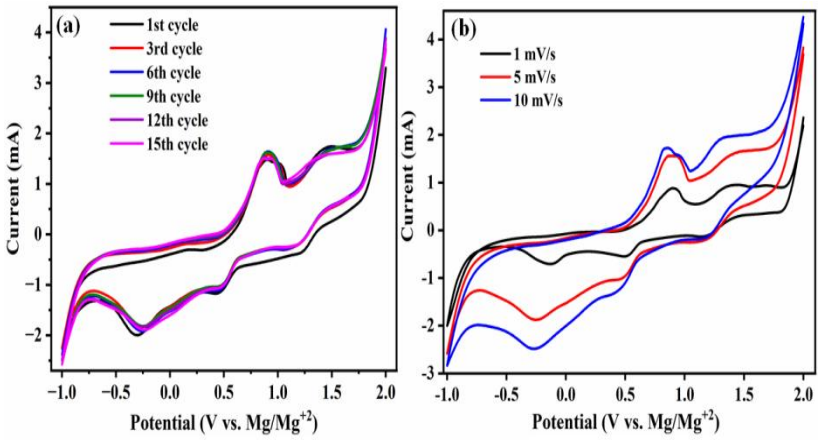

Fig.-3: CV Profiles of Mg-Pt Half-Cell at (a) 5 mV/s Scan Rate, (b) 1, 5, 10 mV/s Scan Rates to Study the Mg Deposition/Dissolution at the Inert Working Electrode

Two-electrode System (Mg/S Battery)

Mg/S cell CV using S@CNTs composite cathode within 0–2.2 V potential window at 5 mV/s scan rate is displayed in Fig.-4a. The CV results reveal a distinct anodic peak at 1.61 V, accompanied by a corresponding cathodic peak at 0.96 V, showing the procedure for intercalation and de-intercalation of Mg ions in the S@CNTs cathode. A pair of broad redox peaks in the forward and reverse direction implies that the electrochemical reduction and oxidation of sulfur occur during charge/discharge, and it is reversible to a greater extent. During the cathodic scans, A noteworthy reduction peak at 0.96 is associated with the generation of higher-order magnesium polysulfides (MgSx, where $4 \leq x < 8$) from elemental sulfur, the subsequent conversion of these polysulfides to lower-order magnesium polysulfides, and finally producing MgS_2 and MgS.[35] During the process of anodic scanning, the oxidation peak that occurs at 1.61 V is connected to the oxidation of MgS_2 and MgS, which then transforms back into the polysulfide MgSx (where $x > 2$). Figure-4b demonstrates the CV of the Mg-S battery at 1, 5, and 10 mV/s scan rates. The cathodic and anodic peaks are shifted to lower and higher potentials, starting at 1 mV/s and going up to 10 mV/s scan rates. The peak current values are stable with the increase in cycle number, which demonstrates the Mg-S cell's electrochemical stability with the S@CNT cathode (Fig.-4a).

The GCD profiles of the Mg-S cell with the S@CNTs cathode at different cycles are illustrated in Fig.-5a. The GCD studies were operated at 0.0 to 2.2 V potential window, at 300 mA/g current density. In the 2nd cycle, the discharge profile reveals a minor discharge plateau, indicating the intercalation of Mg ions into the S@CNTs cathode, with a discharge capacity recorded at 386 mA h/g. With the increase in the cycle life, decay in the capacity was observed, which may be due to the formation of soluble Mg polysulfides and good reversibility. The Mg/S cell containing an S@CNTs cathode exhibits a consistent cycle life of 100 cycles, achieving a capacity retention of 86.5% and the capacities were 386, 386, 360, 353, 334 mA h/g at 2nd, 25th, 50th, 75th, and 100th cycles, respectively, with 95 % coulombic efficiency shown in Fig.-5b. Thus, the results demonstrate that the combination of S@CNTs and novel 0.1 M $BMIMBF_4$+$Mg(TFSI)_2$ electrolyte would be a good choice for Mg/S batteries.

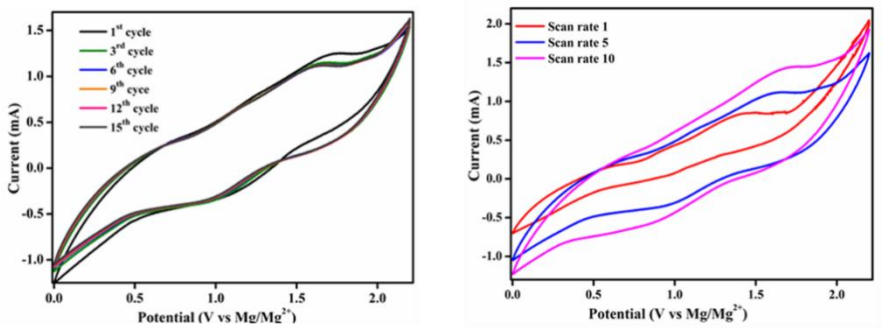

Fig.-4: Mg/S cell CV Curves with S@CNTs Cathode (a) at 5 mV/s Scan Rate for different Cycles, (b) at different Scan Rates (1, 5, 10 mV/s)

Further modifications and detailed studies have to be carried out to achieve better specific capacity and performance of the Mg/S batteries electrochemically. The following equations provide an illustration of the electrochemical reactions that occur in the Mg/S@CNTs battery.[5,35]

$$S_8 + 4e^- + Mg^{2+} \rightarrow 2MgS_4 \quad (1)$$

$$MgS_4 + 2e^- + Mg^{2+} \rightarrow 2MgS_2 \quad (2)$$

$$MgS_2 + 2e^- + Mg^{2+} \rightarrow 2MgS \quad (3)$$

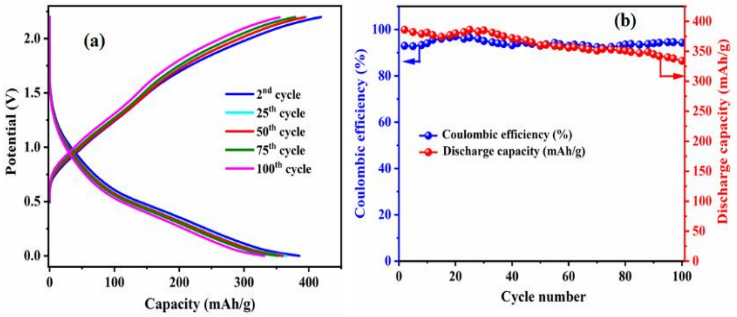

Fig.-5: GCD Profiles of the S@CNTs Cathode in the Mg/S Battery within the Potential Window 0.0 -2.2 V

Post-mortem Analysis

To comprehend the electrochemical mechanisms underlying the Mg/S@CNTs cells during charge-discharge cycling, post-mortem analysis of the cycled S@CNTs cathode was conducted by XPS, UV-Vis, FE-SEM, and EDX analysis. Following 100 GCD cycles, the Mg/S cell was disassembled, and the S@CNTs cathode was retrieved. Cycled S@CNTs rinsed with ethanol for 3-4 times, oven-dried at 70 °C for 12 h.

UV-Vis Analysis

The findings of the UV-Vis analysis of the discharged S@CNTs cathode are shown in Fig.-6. The discharged cathode was submerged in DMSO solvent for 48 h to get the liquid samples. The cycled and pristine S@CNTs electrode exhibits two characteristic absorbance peaks at 310 and 380 nm, respectively.[38] The absorbance peak at about 380 nm corresponds to the presence of S_8^{2-}, observed in both cycled and pristine electrodes. The absorbance peak at 310 nm may be the secondary product produced from S_8^{2-}, i.e., S_6^{2-} or S_4^{2-}[39] which is probably a sign of elemental sulfur dissolution,[40] the UV–Vis spectra demonstrated that during the cycling process, elemental sulfur dissolution appears to be more noticeable compared to the polysulfides present in the electrolytes, indicating not much structural change in the S@CNTs cathode after charge-discharge cyclings.

XPS Analysis of Cycled S@CNT Electrode

After the 100th discharge, the S@CNTs cathode XPS survey spectra show peaks for Mg 1s and Mg 2p, which correspond to Mg, which may be due to MgS_x formation. The peaks corresponding to F (fluorine) and Cl (chlorine) in the XPS survey spectrum could be assigned to the binder as well as specific electrolyte molecules or residues.[5] High-resolution S 2p spectrum (Fig.-7d) demonstrates three prominent peaks.

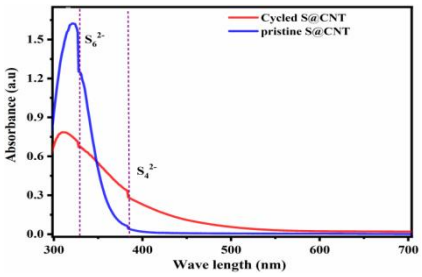

Fig.-6: UV Analysis of Pristine and Cycled S@CNTs Cathode

The peak observed at 160.40 eV is attributed to the Mg-S bond present in both MgS and MgS_2, peak at 164.8 eV (shift of S $2p_{1/2}$ peak of sulfur in composite to lower binding energy) indicates the formation of MgS_x ($1 < x < 8$), and the peak at 166.4 eV at higher binding energy may ascribed to S-O bonds, which may be due to $TFSI^-$ anion of the ionic liquid used.[5, 35]

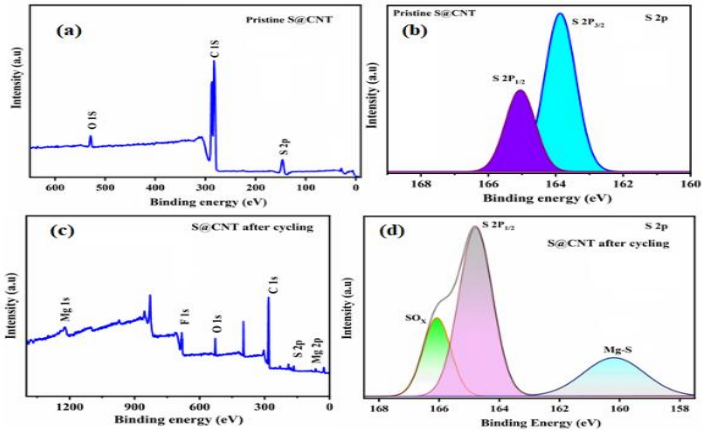

Fig.-7: (a) Pristine S@CNTs Cathode XPS Survey Spectrum, (b) High-resolution S 2p XPS Spectra of Pristine S@CNTs, (c) The S@CNTs Cathode's XPS Survey Spectra over 100 Discharge Cycles, and (d) High-Resolution S 2p XPS Spectra of the S@CNs Cathode after 100 Cycles in the Discharge State

FE-SEM and EDAX cycled S@CNTs electrode

FESEM and EDS of the discharged S@CNTs are shown in Fig.-8. This illustrates the morphology changes in the S@CNTs cathode during the discharge process. After complete discharge, the exterior of the S@CNTs cathode became dense due to the deposition of magnesium sulfides.[41] The FESEM image of cycled S@CNTs cathode maintains its homogenous morphology and porous shape with reduced passive layer development on the surface (Fig.-8a, b).

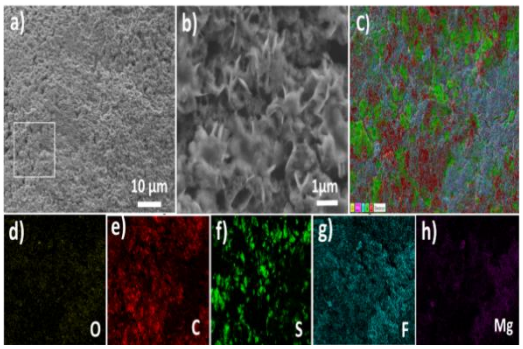

Fig.-8: FESEM Images of Cycled S@CNTs Cathode (a) High (b) Low Magnification (c) EDS and (d-h) Elemental Mapping of Cycled S@CNTs

Figure-8c shows EDX with C, Mg, O, and S distributions in the cycled S@CNTs cathode (after 100 cycles), respectively. The cathode's porous structure facilitates the active material's efficient accessibility to the electrolyte, which in turn promotes the transit of Mg ions to the active sulfur. Elemental mapping

(Fig.-8d-h) shows the presence of Mg along with S and C elements, confirming the insertion and de-insertion of Mg into the cathode during discharge and charge cycles.

Electrochemical Impedance Studies

Figure-9 shows the EIS of the S@CNTs electrode before and after cycling. The two spectrums' shapes are quite close. The semicircle observed in the high-frequency region indicates the presence of contact resistance and charge transfer resistance. A brief sloped line in the low-frequency regions results from ion diffusion occurring within the cathode. The diameter (Fig.-10, black) of the semicircle in pristine S@CNTs is much smaller compared to cycled S@CNTs, which indicates the pristine S@CNTs have lower contact resistance and charge transfer resistance. After 100 cycles, the observed decline in capacity may be attributed to the formation of a solid electrolyte interphase (SEI) within the cycled S@CNTs cathode. With repeated cycling, the depth of the SEI layer increased, creating an obstacle to Mg^{2+} ion migration. The presence of a blocking interface on the Mg surface leads to irregularities in the Mg stripping and plating processes, which influence battery performance and reliability. Magnesium Sulfide (MgS_2 or MgS) undergoes a bidirectional process during charge-discharge.

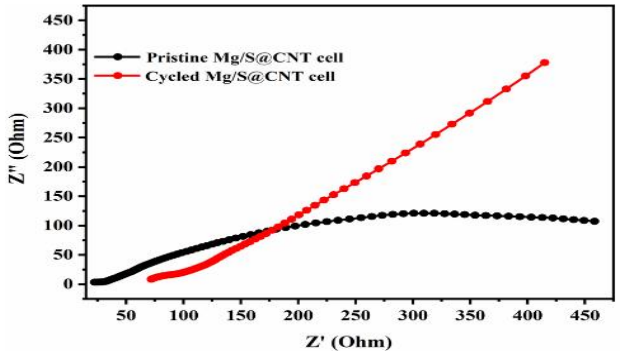

Fig.-9: EIS Spectra of the S@CNTs Electrode Before (black line) and after (red line) the Charge-Discharge Cycles

The S@CNTs cathode revealed its electrochemical performance, recording a reversible discharge capacity of 386 mA h/g after completing 100 cycles at 334 mA/g. The sulfur electrode's porous carbon (MWCNTs) structure is crucial for improving electrochemical performance in 0.10 M /$BMMIBF_4$+$Mg(TFSI)_2$ electrolyte. In addition to raising the composite's electrical conductivity, a favorable carbon makes it easier for Mg-ions to move throughout the structure. The development of a safe, dendrite-free Mg/S cell, which relies on the abundant resources of Mg and S, will make it a formidable competitor to current rechargeable technologies for large-scale applications. Nevertheless, a lot of work needs to be done to make the Mg/S system a practical energy-storage technology.

CONCLUSION

In conclusion, we successfully synthesized the S@CNTs composite utilizing a simple, affordable, and eco-friendly process. The best cathode sorbent is porous carbon (CNT) because it has a high adsorption capacity and strong conductivity. MWCNTs were used as sulfur hosts/confinements to create carbon-supported sulfur cathodes by the melt-diffusion technique. The Mg/S battery with S@CNTs, Mg, 0.10 M $Mg(TFSI)_2$/$BMIMBF_4$ performed well in terms of cyclic stability (100 cycles) and rate capability, with a high capacity of 386 mA h/g with 86.5 % capacity retention and 95 % coulombic efficiency. MWCNTs assist in maintaining electrode structure throughout the cycling and provide several ionic and electrical channels for rapid discharge-charge. Polysulfide ion dissolution is suppressed, and active material dissolution is minimized due to the characteristics of the ionic liquid electrolyte. A dendrite-free, safe Mg/S cell utilizing plentiful Mg and S will be very competitive with existing rechargeable advancements for large-scale applications.

ACKNOWLEDGEMENTS

S.R. wishes to acknowledge the Council of Scientific and Industrial Research (CSIR), India, for financial assistance in the form of a Senior Research Fellowship, Academy of Scientific and innovative research (AcSIR), and CSIR-IICT for the Ph.D. Also acknowledges the help extended by Y.S. Latha, Alock,

Anitha, Dr M. Latha, and the Dr.JVR group, who have strong support. The authors thank the Director, CSIR-IICT (Ms.no.IICT/Pubs./2024/220).

CONFLICT OF INTEREST

The authors declare that they have no known competing financial interests or personal relationships that could have appeared to influence the work reported in this paper.

AUTHOR CONTRIBUTIONS

The present work is related to *SDG-7: Affordable and Clean Energy*. All the authors contributed significantly to this manuscript, participated in reviewing/editing and approved the final draft for publication. The research profile of the authors can be verified from their ORCID ids, given below:

Sake Rayamma https://orcid.org/0009-0006-2509-3233
Jetti Vatsala Rani https://orcid.org/0000-0003-4761-6198
Latha Malyala https://orcid.org/0000-0002-9930-3954

REFERENCES

1. Yanlu, Cong wang, Qiang Liu, Xiaoyan li, Xinyu Zhao, and Zaiping Guo, *Small methods,* **5**, 2001303 (2021), https://doi.org/10.1002/smtd.. 202001303
2. Wenwen Liu, Xingbin Yan, Junwei Lang, and Qunji Xue, *Journal of Materials Chemistry*, **22**, 8853(2021), https://doi.org/10.1039/c2jm15537k
3. J.T.S. Irvine, *Journal of Power Sources*, **136,** 203(2007), https://doi.org/10.1026/j.jpowsour.2004.03.002
4. Y. Q. Sun, Q. Wu and G. Q. Shi, *Energy and Environmental Science*, **4**, 1113(2011), https://doi.org/10.1039/c0ee00683a
5. Vinayan, B. P, Zhirong Zhao-Karger, Thomas Diemant, Venkata Sai Kiran Chakravadhanula, Nele I. Schwarzburger, Musa Ali Cambaz, R. Jürgen Behm, Christian Kübel, and Maximilian Fichtner, *Nanoscale*, **8**, 3296(2016), https://doi.org/10.1039/c5nr04383b
6. T. D. Gregory, R. J. Hoffman and R. C. Winterton, *Journal of the Electrochemical Society*, **137**, 775(1990), https://doi.org/10.1149/1.2086553
7. H. S. Kim, T. S. Arthur, G. D. Allred, J. Zajicek, J. G. Newman, A. E. Rodnyansky, A. G. Oliver, W. C. Boggess, and J. Muldoon, *Nature Communications,* **2**, 427(2011), https://doi.org/10.1038/ncomms1435
8. Manthiram, Arumugam, Yongzhu Fu, and Yu-Sheng Su, *Accounts of Chemical Research,* **46(5)**, 1125*(2013)*, https://doi.org/10.1021/ar300179v
9. Wang L, Riedel S.Drews, J, and Zhao-Karger Z, *Frontiers in Batteries and Electrochemistry,* **3,** 358199(2024), https://doi.org/10.3389/fbael.2024.1358199
10. X. Yu, A. Manthir, *Advanced Functional Materials,* **30**, 2004084(2020), https://doi.org/0.1002/adfm.. 202004084
11. Zhirong, ZK. Maximilian, F. *MRS Communications* **7**, 770(2017), https://DOI:.org/10.1557/mrc.2017.101
12. L Sheng, J Feng, M Gong, L Zhang, J Harding, Z Hao, FR.Wang, *Molecules* **29(6),** 1234(2024), https://doi.org/10.3390/molecules29061234
13. Zhao-Karger, Z, Liu, R, Dai, W, Li, Z, Diemant, T, Vinayan, B. P, and Fichtner, M, ACS Energy Letters, **3(8)**, 2005(2018**),** https://doi.org/10.1021/acsenergylett.. 8b01061
14. Kong, Long, Chong Yan, Jia-Qi Huang, Meng-Qiang Zhao, Maria-Magdalena Titirici, Rong Xiang, and Qiang Zhang, *Energy and Environmental Materials,* **1**, 100(2018), https://doi.org/10.1002/eem2.12012

15. Tian, Shuanbao, Yanhong Yin, Zhaoxia Cao, Hongyun Yue, and Shuting Yang, *Ionics,* **24,** 33(2018), https://doi.org/10.1007/s11581-017-2165-z
16. Huang JQ, XU ZL, Sara A, *Carbon,* **99,** 624(2016), https://doi.org/10.1016/j.carbon.2015.12.081
17. Jiang, Y., Lu, M, Ling, X., Jiao, Z., Chen, L., and Zhao, B., *Journal of Alloys and Compounds,* **645**, 509(2015), https://doi.org/10.1016/j.jallcom.2015.05.125
18. D. Wang, Da-Wei, Qingcong Zeng, Guangmin Zhou, Lichang Yin, Feng Li, Hui-Ming Cheng, Ian R. Gentle, and Gao Qing Max Lu, *Journal of Materials Chemistry A,* **1**, 9382(2013), https://doi.org/10.1039/c3ta11045a
19. Yang, Yuan, Guangyuan Zheng, and Yi Cui. *Chemical Society Reviews,* **42**, 3018(2013), https://doi.org/10.1039/c2cs35256g
20. Cheng, Xin-Bing, Jia-Qi Huang, Qiang Zhang, Hong-Jie Peng, Meng-Qiang Zhao, and Fei Wei, *Nano Energy,* **4**, 65(2014), https://doi.org/10.1016/j.nanoen.2013.12.013
21. Vinayan, Bhaghavathi P, Holger Euchner, Zhirong Zhao-Karger, Musa Ali Cambaz, Zhenyou Li, Thomas Diemant, R. Jürgen Behm, Axel Gross, and Maximilian Fichtner, *Journal of Materials Chemistry A,* **7**, 25490(2019), https://doi.org/10.1039/c9ta09155f
22. Swapnil A. Dharaskar, Kailas L. Wasewar, Mahesh N.Varma, Diwakar Z. Shende, Changkyoo Yoo, *Arabian Journal of Chemistry,* **9**, 578(2016), https://doi.org/10.1016/j.arabjc.2013.09.034
23. Yanna Nu Li, Jun Yang, Rong Wu, *Electrochemistry Communications,* 7, 1105(2005), https://doi.org/10.1016/j.elecom.2005.07.013
24. Kim, Seok, Yongju Jung, and Soo-Jin Park, *Journal of Power Sources,* **152**, 272(2005), https://doi.org/10.1016/j.jpowsour.2005.03.003
25. S. Kim, Y. Jung, and S. J. Park, *Electrochimica Acta,* **52**, 2116(2007), https://doi.org/10.1016/j.electacta.2006.08.028
26. N. Amir, Y. Vestfrid, O. Chusid, Y. Gofer, D. Aurbach, *Journal of Power Sources* **174**, 1234(2007), https://doi.org/10.1016/j.jpowsour.2007.06.206
27. Wang, Pu, Yanna NuLi, Jun Yang, and Zhenzhen Feng, *Surface and Coatings Technology,* **201(6),** 3783(2006), https://doi.org/10.1016/j.surfcoat.2006.03.020
28. Shterenberg, Ivgeni, Michael Salama, Hyun Deog Yoo, Yosef Gofer, Jin-Bum Park, Yang-Kook Sun, and Doron Aurbach, *Journal of The Electrochemical Society*, **162(13),** A7118(2015), https://doi.org/10.1149/2.0161513jes
29. Swapnil A. Dharaskar a, Kailas L. Wasewar, Mahesh N. Varma, Diwakar Z. Shende, ChangKyoo Yoo, *Arabian Journal of Chemistry*, **9(4)**, 578(2016), https://doi.org/10.1016/j.electacta.2006.08.028
30. Jia-Jia, Chen, Jia Xin, She Qiu-Jie, Wang Chong, Zhang Qian, Zheng Ming-Sen, and Dong Quan-Feng, *Electrochimica Acta*, **55**, 8062(2010), https://doi.org/10.1016/j.electacta.2010.01.069
31. Jiang, Weichuan, Yinghui Bian, Yonglei Zhang, and MengChang Lin, *IOP Conference Series: Earth and Environmental Science,* **692,** 032070(2021), https://doi.org/10.1088/1755-1315/692/3/032070
32. Xiao, Qinghuiqiang, Jinlin Yang, Xiaodong Wang, Yirui Deng, Peng Han, Ning Yuan, Lei Zhang, Ming Feng, Chang-an Wang, and Ruiping Liu, *Carbon Energy*, **3**, 271(2021), https://doi.org/10.1002/cey2.96
33. Su, Yu-Sheng, Yongzhu Fu, and Arumugam Manthiram, *Physical Chemistry Chemical Physics,***14**, 14495(2012), https://doi.org/10.1039/c2cp42796f
34. Xin, Sen, Lin Gu, Na-Hong Zhao, Ya-Xia Yin, Long-Jie Zhou, Yu-Guo Guo, and Li-Jun Wan, *Journal of the American Chemical Society*, **134(45)**, 18510(*2012*), https://doi.org/10.1021/ja308170k
35. Z. Zhao-Karger, X. Y. Zhao, D. Wang, T. Diemant, R. J. Behm, and M. Fichtner, *Advanced Energy Materials*, **5,** 1401155 (2014), https://doi.org/10.1002/aenm.. 201401155
36. Wang, Zhiyu, Yanfeng Dong, Hongjiang Li, Zongbin Zhao, Hao Bin Wu, Ce Hao, Shaohong Liu, Jieshan Qiu, and Xiong Wen Lou, *Nature Communications*, **5(1)**, 5002(2014), https://doi.org/10.1038/ncomms6002

37. Li Guoxing, Jinhua Sun, Wenpeng Hou, Shidong Jiang, Yong Huang, and Jianxin Geng, *Nature Communications*, **7(1),** 10601 (2016), https://doi.org/10.1038/ncomms10601
38. R. Martin, Robert P., William H. Doub Jr, Julian L. Roberts Jr, and Donald T. Sawyer, *Inorganic Chemistry,* **12 (8),** 1921(1973), https://doi.org/10.1021/ic50126a047
39. Kim, Bum-Soo, and Su-Moon Park, *Journal of the Electrochemical Society,* **140(1),** 115(1993), https://doi.org/10.1149/1.2056070
40. Cañ as, Natalia A, David N. Fronczek, Norbert Wagner, Arnulf Latz, and K. Andreas Friedrich, *The Journal of Physical Chemistry C,* **118 (23),** 12106(2014), https://doi.org/10.1021/jp5013208
41. S.C. Han, M.S. Song, H. Lee, H.S. Kim, H.J. Ahn, J.Y. Lee, *Journal of the Eectrochemical Society*,**150** (7), A889(2003), https://doi.org/10.1149/1.1576766
42. Han, Sang-Cheol, Min-Sang Song, Ho Lee, Hyun-Seok Kim, Hyo-Jun Ahn, and Jai-Young Lee, *Journal of the Electrochemical Society*, **150(7),** A889(2003), https://doi.org/10.1149/1.1576766

[RJC-9278/2025]